Available online at https://ifejost.oauife.edu.ng

IFE JOURNAL OF SCIENCE AND TECHNOLOGY

Vol 9. No. 1 (2025) 13 –33

CHITOSAN-PORPHYRIN COMPOSITE (CPC) AS PHOTOSENSITIZER IN ANTIBACTERIAL PHOTODYNAMIC THERAPY FOR THE MANAGEMENT OF CHRONIC WOUNDS

Reama Chinedu George[1], Afusat Ajoke Olajide[1], Oluwafemi Bamidele Daramola[2,3*], Nkem Torimiro[3]

[1]Department of Chemistry, Obafemi Awolowo University, Ile-Ife, 220005, Nigeria

[2]Department of Microbiology, Osun State University, Osogbo, 210001, Nigeria
[3]Department of Microbiology, Obafemi Awolowo University Ile-Ife, 220005, Nigeria

*Correspondence: oluwafemidaramola8@gmail.com

Abstract
A promising method to prevent and control infections is Antimicrobial Photodynamic Therapy (APDT). This study investigated the use of chitosan-porphyrin composite (CPC) as photosensitizer for APDT test against four wound bacterial isolates: *Staphylococcus aureus, Klebsiella pneumonia, Proteus mirabilis,* and *Escherichia coli*. The chitosan extracted from fresh prawns and porphyrins with different functional groups complexed with zinc, tin, and silver were used. The functional groups on the porphyrin were 4-phenyl (TPP), 4-sulphonatophenyl (TPPS), 4-hydroxylphenyl (THPP), 4-carboxylphenyl (TCPP), 4-methoxylphenyl (TMPP), 4-methyl-4-pyridyl (TMPyP). The CPCs were characterized using UV-Vis and Infra-red spectroscopic techniques and the results confirmed weak interactions between the chitosan and porphyrin molecules and in some cases resulting in aggregation of the porphyrin molecules. A screening study was conducted to investigate both the dark toxicity and photo-toxicity of the composites using agar well diffusion method. The composites that displayed growth inhibition against all pathogens underwent additional evaluation to determine their minimum inhibitory concentration (MIC), minimum bactericidal concentration (MBC), and killing rates. The study found that only silver *meso*-tetra(4-methoxylphenyl)porphyrin-chitosan composite (C-AgTMPP) and silver *meso*-tetra(4-hydroxylphenyl)porphyrin-chitosan composite (C-AgTHPP) among the twenty-eight CPCs showed activity against all the pathogens, with MBC values as low as 1.25 ug/mL and eradicating the pathogens within 24 hours of exposure to light.

Keywords: APDT, Chitosan, Chitosan-Porphyrin Composites, Photosensitizers, Wound.

INTRODUCTION

A wound that takes longer to heal than expected is considered a chronic wound and always necessitates therapeutic intervention to facilitate the healing process (Zhu *et al*., 2017). Examples of such wounds include diabetic foot ulcers, venous leg ulcers, burn victim wounds, and pressure sores. In some cases, certain disease conditions contribute to the chronicity of wounds, such as malnutrition, cancer, radiation injury, diabetes mellitus, and chronic diseases like renal disease (Harding, *et al*., 2002). These patients are most likely to have suppressed immunity, rendering their bodies unable to fight infections and creating an environment favourable for bacterial colonization of the wound. *Pseudomonas aeruginosa* (Gram-negative) and *Staphylococcus aureus* (Gram-positive) are the primary bacteria that infect an open wound within the first 24-48 hours and after a week, other bacteria such as *Proteus mirabilis, Klebsiella pneumoniae,* and *Escherichia coli* with increased antibiotic resistance may also be found (Abbaspour *et al*., 2015).

Preventing infections in chronic wounds is crucial for successful wound healing; however, effectively managing persistent and festering wounds to achieve timely healing remains a significant challenge for traditional and modern medical practitioners. Common methods used to prevent or control wound infections include wound cleaning, debridement, and antibiotic therapy (topical and/or systemic) (Atiyeh *et al.,* 2009). More advanced techniques involve using specialized dressings like foam dressings, hydrocolloids, hydrogels, alginate dressings, and films, as well as treatments like negative pressure wound therapy (NPWT), hyperbaric oxygen therapy (HBOT), bioengineered skin substitutes, platelet-rich plasma (PRP) therapy, growth factors and cytokines, electrical stimulation, compression therapy, and surgical interventions (Okur *et al*., 2020; Zhang *et al*., 2020; Hoang *et al*., 2022; Ongarora *et al*., 2022). However, these methods can be expensive and may not be readily available in low-income areas. Some procedures require anaesthesia, and the use of antibiotics alongside NPWT, HBOT, and PRP is considered supplementary to the commonly used methods.

Therefore, there is a need to find more affordable and effective dressings/treatments for managing chronic wounds, and antibacterial photodynamic therapy (APDT) holds promise in this regard. APDT is a non-invasive therapy that utilizes three components: a photosensitizer (PS), light, and oxygen to inactivate pathogens (Kou *et al*., 2017). It employs molecular oxygen as the neighbouring molecule, absorbing energy from an excited PS to form cytotoxic chemical species that cause the "photo-killing" of bacteria upon illumination with ultraviolet and visible light rays. The administered photosensitizers, which are dye molecules, can be absorbed either into the cells of the microbes or on the surface of the cell wall. Initially, the photosensitizers are in the ground singlet state ($^1PS_0$) before exposure to light. Upon light irradiation, they absorb photons of a specific wavelength (i.e. the visible region and may extend to the near-infrared region) (Karaoğlu *et al.*, 2020; Almenara-Blasco *et al*., 2024) and undergo transition to an excited singlet state ($^1PS_{exc}$). This excited singlet state can follow two pathways - it can either radiatively decay to the ground state, resulting in fluorescence, or undergo intersystem crossing (ISC), leading to the formation of the triplet state (^3PS). The triplet excited state has lower energy and a longer lifetime (10^{-3} s). The excited state dynamics of the PS has been summarized in Figure 1. In the triplet state, the photosensitizer interacts with the surrounding molecules through two types of photochemical reactions, known as Type I and Type II, which produce various cytotoxic reactive oxygen species (ROS) (Ongarora *et al*., 2022). Both Type I and Type II reactions are oxygen-dependent and are believed to occur simultaneously during antimicrobial photodynamic therapy (APDT), requiring proximity between the ^3PS and molecular oxygen (Ormond and Freeman, 2013).

APDT offers several advantages over other antibacterial therapies. It is non-invasive and targets various structures within the pathogen, which could alter the different metabolic pathways of the microorganism, unlike the other treatments (Feese *et al*., 2011).

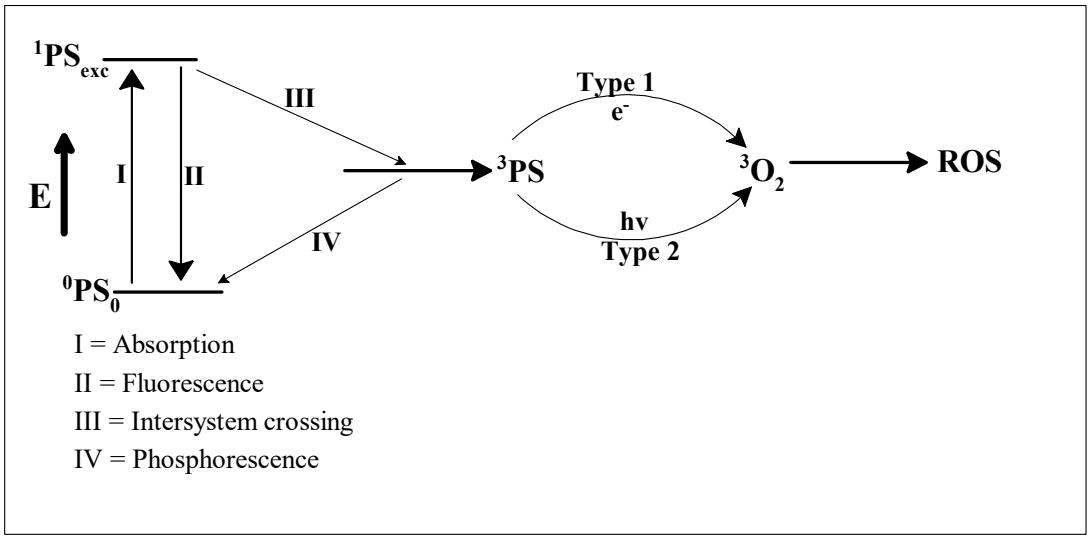

Figure 1: Photochemical reactions mechanism of ROS generation by photodynamic therapy (Kou *et al*., 2017).

The process occurs so rapidly that the microorganism does not have sufficient time and resources to recover and engage in adaptive survival mechanism. It also disables the pathogens' ability to develop cross-generational adaptivity mechanisms against the therapy (Feese *et al*., 2011; Ranjbar and Takhtfooladi, 2016). Additionally, the other components of this therapy, oxygen and light, are non-toxic, and are freely available in nature, making the therapy effective for localized infected wound such as chronic sores. Typically, dyes used as PSs in APDT are tetrapyrrole based (i.e. porphyrinoids), coordinated to a wide range of metal ions. Examples include chlorins, bacteriochlorins, phthalocyanines, and porphyrins. Non-porphyrinoids such as methylene blue, rose bengal, toluidine blue O, neutral red, fullerenes, naturally occurring curcumin, and hypericin have also been used (Voila and Dall'Acqua, 2006; Vilela *et al*., 2012; Prasanth *et al*., 2014; Shrestha *et al*., 2015). An ideal ADPT photosensitizer should be able to absorb light within the phototherapeutic spectral window, ranging from 600 to 850 nm, and generate a high quantum yield of its triplet state (Karaoğlu *et al.*, 2020; Almenara-Blasco *et al*., 2024). High chemical purity, thermal stability at room temperature, ease of penetration into the cell wall of the bacteria, and high photostability, are among other essential characteristics of an ideal PS (Král *et al*., 2000; Ormond and Freeman, 2013).

Extensive research has been conducted on the use of porphyrins as photosensitizers in APDT (Milanesio *et al*., 2001; Caminos *et al.,* 2008; Liu et al., 2015; Gyulkhandanyan *et al*., 2016; Fayyaza *et al*., 2016; Gourlot *et al*., 2022; Savelyeva *et al.,* 2023; Ji *et al.,* 2023; Zhang *et al*., 2024). Porphyrins are macrocyclic compounds made up of four pyrrole rings bonded together by methine bridges. They possess an extensive conjugated π system with 22-π-electrons, of which 18 are delocalized. These compounds absorb light in the UV-Vis region of the electromagnetic spectrum due to their conjugated π system, resulting in a variety of electronic and optical properties (Gouterman, 1978). Porphyrins generate long-lived triplet states, especially when metals have been inserted into the porphyrin ring (Gouterman, 1978). In the triplet state, they effectively transfer energy to the surrounding molecular oxygen ($^3O_2$), generating a high singlet oxygen quantum yield, which is the cytotoxic agent that is responsible for the death of the bacteria (Bonnett *et al.,* 1988). They are also easily synthesized from readily available precursors, easy to replicate and functionalize, allowing tuning of their absorption bands to absorb light in the visible region and near infrared, and can be made water-soluble by introducing charged substituents (Woodburn *et al*., 1994; Tominaga *et al*., 1997). These unique properties make porphyrins ideal as PSs for APDT compared to other dyes.

Currently, the major drawback with application of porphyrin in APDT is the loss of antimicrobial activity of PS molecules through leaching (Feese *et al.,* 2011) and inadequate uptake of PSs by

bacteria, resulting in insufficient photosensitization (Lui *et al*., 2015). Studies have shown that structural modifications of existing PSs, including immobilization of PSs on biopolymeric material, have optimized APDT efficacy, and chitosan and cellulose have been investigated (Huang *et al.,* 2010; Feese *et al.,* 2011; Buchovec *et al*., 2016). Tsai *et al.* (2011) investigated the photodynamic inactivation (PDI) of hematoporphyrin (Hp) combined with chitosan efficacy against *Acinetobacter baumannii*, *Pseudomonas aeruginosa, Staphylococcus epidermidis, Staphylococcus pyogenes*, and methicillin-resistant *Staphylococcus aureus* (MRSA). Feese *et al.* (2011) used cellulose nanocrystals with surfaces modified with cationic porphyrins to photodynamically inactivate *Mycobacterium smegmatics* and *Staphylococcus aureus*. Shrestha *et al.* (2012) studied the efficacy of rose bengal when immobilized on chitosan against *E. faecalis* and *P. aeruginosa*.

Chitosan is a modified natural biopolymer derived from chitin. Chitin is a biopolymeric substance found in the exoskeleton of invertebrate marine animals, insects, fungi, and yeast, with the largest source being crustaceans such as snails, shrimp, crabs, etc. Chitin $(C_8H_{13}O_5N)_n$ is a linear polysaccharide made up of repeated units of single sugar monomer *N*-acetyl-glucosamine linked together via *β*-1,4 bonds. This polymer is biodegradable, biocompatible, non-toxic, and environmentally friendly, with some antioxidant, anticancer, and antimicrobial properties against bacteria, fungi, and yeast (Majekodunmi, 2016). As a result, it is extensively studied, especially for medical and pharmaceutical applications (Tsai and Su, 1999; Raafat *et al*., 2008; Majekodunmi, 2016).

In our recent study, a series of porphyrins (Figure 2), were synthesized and characterized, and the effects of functional groups and metal ions on APDT were investigated (Daramola *et al.,* 2021; George *et al.,* 2022). This study capitalized on the advantages offered by each of the components of the composite material (chitosan-porphyrin composite (CPC)) to achieve enhanced antibacterial activity. To the best of our knowledge, there are no studies on the application of chitosan-porphyrin composites against the selected Gram-negative (*Klebsiella pneumoniae, Proteus mirabilis, Escherichia coli*) and Gram-positive bacteria (*Staphylococcus aureus*). These strains are the most predominant pathogens found in wounds and are equally reported as multidrug-resistant pathogens (Alves *et al*., 2009; Abrahamse and Hamblin, 2016).

It is expected that the synergistic combination of the porphyrin derivatives with the antimicrobial ability of chitosan could lead to an enhanced inactivation of these Gram-positive and Gram-negative bacteria in the presence and absence of light.

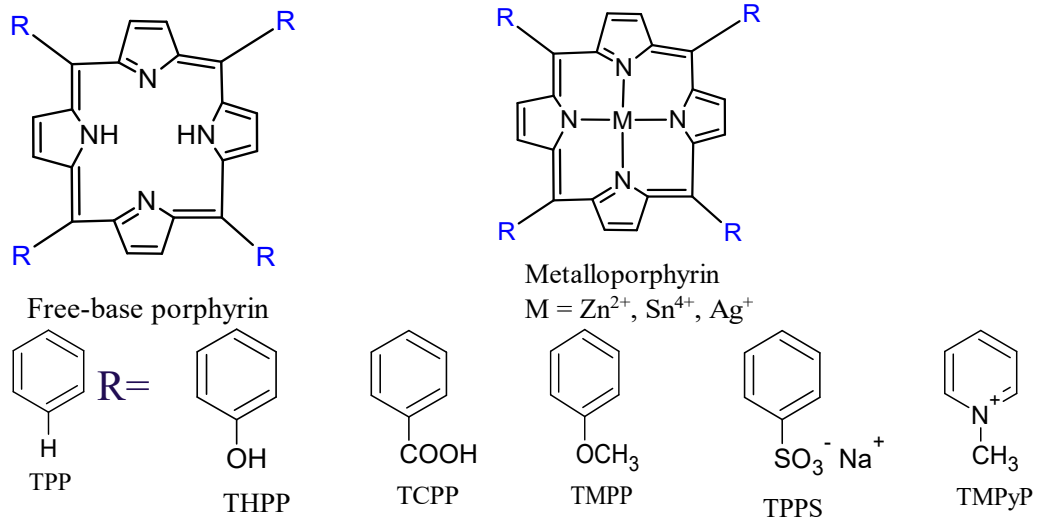

Figure. 2: Chemical structure of the studied porphyrin molecules.

MATERIALS AND METHODS

All reagents and solvents used for this study were purchased from Merck and Sigma Aldrich and used without further purification. Fresh prawns (*Dendrobranchiata* Family) used in this study were obtained from local market. UV-Vis spectra were recorded on a Shimadzu UV–200 spectrophotometer using a path length of 1 cm quartz cells. The electronic spectra were plotted using OriginPro 7.0 software (USA) installed on a personal computer. Fourier Transform Infrared (FT-IR) (4000–400 cm^{-1}) was recorded on a KBr disk Shimadzu FT–IR 8400). The incubator used was Gallenkamp, UK. Auto colorimeter (Metzer, India) at 540 nm and Mueller-Hinton agar (MHA) plates were used for the antibacterial studies.

Preparation of Chitosan–Porphyrin Composite (CPC)

The preparation of CPC is in two stages - first is the extraction of chitin and its conversion to chitosan. The second is, the immobilization of the porphyrin on chitosan. The chitosan employed in this study was formed by alkaline hydrolysis of chitin as reported in the literature with only minor modification (Majekodunmi, 2016). In this procedure, deproteination was performed first by treating with 4% NaOH for 24 hours, followed by demineralization using 4% HCl for 12 hours. Decolourization was carried out with 1% oxalic acid for 30 minutes. The deacetylation process involved treatment with 65% NaOH for 3 days.

Extraction of Chitin and its Conversion to Chitosan

The shells of fresh prawns (500 g) were removed from the flesh and washed with warm water. Thereafter they were sun-dried and ground to powder. The powdered shells (24 g) were subjected to demineralization, deproteination, and deacetylation as illustrated in Figure 3.

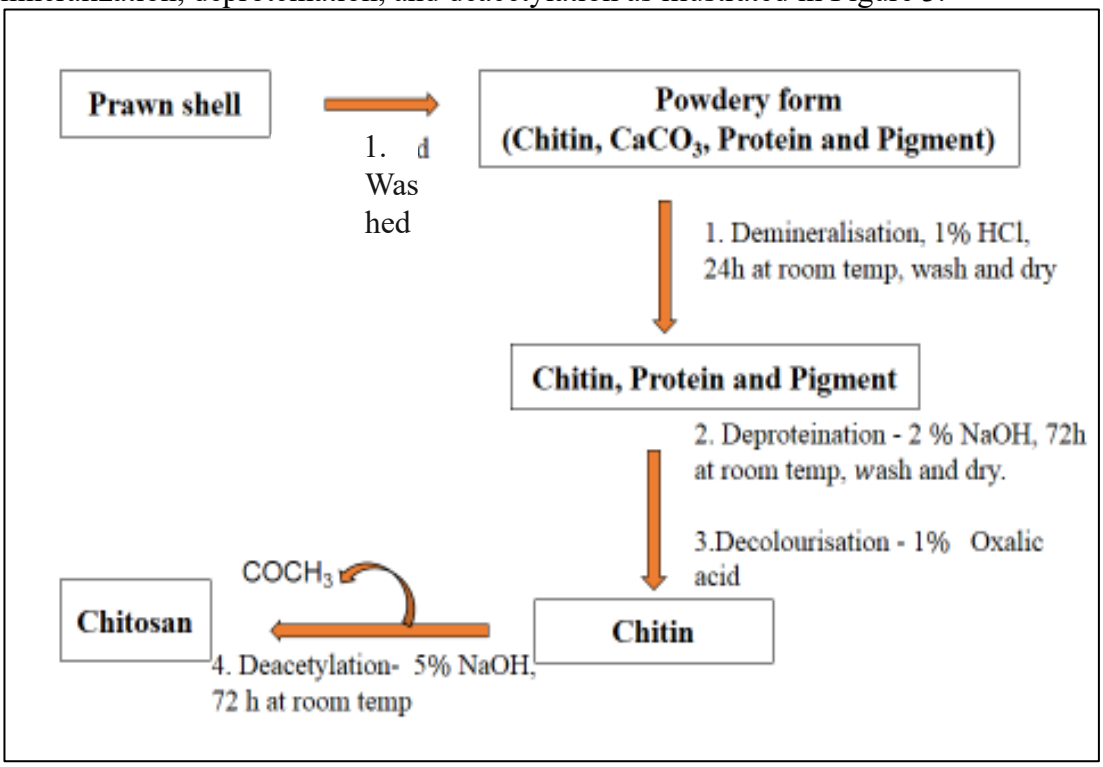

Figure 3: Flow chart showing the steps taken for the preparation of chitosan

The chitin and chitosan were characterized using FT-IR spectroscopy and the degree of deacetylation (DDA) of chitosan was calculated using the baseline proposed by Domszy and Roberts (2010). The computation equation for the baseline is given by Equation 1:

$$DDA\ \% = 100 - \left[\left(\frac{A_{1655}}{A_{3450}}\right) \times \frac{100}{1.33}\right] \quad (1)$$

where A_{1655} and A_{3450} are the absorbances at 1655 cm^{-1} for the primary amide (1° amide) band and 3450 cm^{-1} is for the hydroxyl band. The absorbance of the 1° amide is a measure of the *N*-acetyl group content while the hydroxyl band is an internal standard to correct for film thickness. The factor ′1.33′ denotes the value of the ratio of A_{1655} /A_{3450} for completely *N*-acetylated chitosan.

Fixation of Porphyrins on Chitosan

All the porphyrin molecules were prepared from the condensation reaction of pyrrole with an aldehyde-bearing functional groups of interest (Figure 2). The synthesis and characterization of porphyrins used in this work have been reported in a previous study (Daramola *et al.,* 2021; George *et al.,* 2022). The porphyrins used were *meso*-tetra(4-phenyl) porphyrin (TPP), *meso*-tetra(4-sulphonatophenyl) porphyrin (TPPS), *meso*-tetra(4-hydroxylphenyl) porphyrin (THPP), *meso*-tetra(4-carboxylphenyl) porphyrin (TCPP), *meso*-tetra(4-methoxylphenyl) porphyrin (TMPP) and *meso*-tetra(4-methyl-4-pyridyl) porphyrin (TMPyP). Each of these was metallated with zinc, silver, or tin to obtain their metallated derivatives.

The chitosan-porphyrin composites were prepared according to the method of Castro *et al*., (2019). The solution of each porphyrin (0.5 mmol in 25 mL THF) was mixed with 10 mL of chitosan (0.2 g in 10 mL of 1% acetic acid) and stirred for 15 min at room temperature. 10 mL of distilled water was added resulting in a colloidal solution which was stirred for another 6 hours at 60 °C. Afterward, the mixture was filtered, the residue rinsed repeatedly with distilled water, and then oven-dried to yield the chitosan-porphyrin composite. These were characterized using UV-Vis and FTIR spectroscopy.

Dark- and Phototoxicity of CPC on Microorganisms

Quality Control Analysis

A screening study was carried out using the Agar Well-Diffusion method (Gyulkhandanyan *et al*., 2016) following the same procedure applied in a previous study (George *et al*., 2022). The working concentration was 30 mg of the CPC dissolved in 1 mL of solvent (deionized water and methanol) and 0.3 mL was dispensed into one of the four agar wells drilled on the seeded Mueller-Hinton Agar (MHA) plates for each test bacterial isolate. As a positive control, streptomycin sulphate (84 mg/mL) was added to one of the wells, while sterile distilled water was used as a negative control. Additionally, the solvent used to dissolve CPC was added to the fourth well.

The phototoxicity study involved exposing the content of the plates to a 100-Watt tungsten light source placed approximately 35 cm away. To minimize the effects of infrared rays (heat), a glass tray filled with water was placed between the lamp and the plates. The plates were incubated at 37 ℃ for 24 hours. A second set was incubated in the dark (dark toxicity) for the same duration of time and at the same temperature. The diameters of the zones of inhibition were measured to assess the toxicity of CPC against the Gram-positive and Gram-negative bacteria.

Minimum Inhibitory Concentration (MIC), Minimum Bactericidal Concentration (MBC), and Killing Rates

These were determined for the samples that gave the optimal APDT activity after the quality control analysis i.e. the PS that exhibited APDT activity against all four pathogens. Therefore, SnTCPP, SnTHPP, ZnTCPP, ZnTHPP, and ZnTPPS were included in this aspect of the study for comparison. To determine the MIC and MBC of the active PS, various concentrations of the PSs (1.25, 2.5, and 5.0 µg/mL) were suspended in test tubes containing 4 mL of freshly prepared tryptic soy broth (TSB). Thereafter, 500 µL of the standardized bacterial isolates were inoculated into corresponding broths and gently mixed by shaking. The tubes were incubated under the lamp rays for 18 – 24 hours. After incubation, 100 µL of the cultured suspensions were spread-plated on nutrient agar and were checked for visible growth. The least concentration without growth was recorded as the MBC while concentrations preceding the MBC concentration with slight growth were reported as the MIC. Un-inoculated TSB was prepared as positive control while TSB

inoculated with the respective bacterial isolates but without PSs were used as negative control (Andrew, 2001).

Varying concentrations identified as MBC for each porphyrin compound were assessed for its time-kill assay. The reported MBC for the compounds were introduced in test tubes containing 4 mL TSB. A 500 µL of the standardized bacterial isolates were inoculated into their respective medium and concentrations. The tubes were incubated under the lamp rays for 24 hours. Samples were withdrawn at intervals of 6 hours to determine their killing rates. At those intervals, 100 µL of the suspension broths were withdrawn and serially diluted (1:100). Thereafter, 1000 µL of the dilutions were spread–plated on nutrient agar and incubated at 37 °C for 18 – 24 hours in the dark. Visible growths on the cultured plates were counted and recorded (Alshareef, 2021). The data obtained were statistically analyzed and expressed as mean ± standard deviation (SD) using the statistical software GraphPad Prism version 6.01.

RESULTS AND DISCUSSION

Molecular Characterization

Chitosan

The white crystalline solid chitosan obtained was insoluble in organic solvents and water but soluble in 1% acetic acid solution. The $-NH_2$ group gets protonated by the acetic acid forming a charged species ($-NH_3^+$), enhancing the solubility of chitosan. Hence, the solubility test was used as a preliminary test in the work to confirm the formation of chitosan. Both the chitin and chitosan are UV-Vis inactive because they are largely composed of *N*-acetylglucosamine units resulting in limited UV-Vis absorbance capability. Structural changes were determined from FT-IR spectra of the chitin and chitosan (Supplementary Information, (SI-1)) and the significant bands of chitin and chitosan are summarized in Table 1.

It is not unexpected that not all the chitin was converted to chitosan, accounting for the presence of the N–H and C=O bands in the chitosan IR spectrum (Zvezdova, 2010). The bands at 1562 and 1659 cm^{-1} were assigned to N–H bending vibration and C=O stretching vibration respectively, from $–NHCOCH_3$ in chitin which were also present in chitosan but at a slightly lower wavenumber. According to other reports, an increase in the N–H band intensity with a corresponding decrease in the C=O band intensity is indicative of effective deactylation as well as prevalence of the $–NH_2$ groups (Zvezdova, 2010).

Table 1: FT-IR data of chitin of chitosan (KBr cm^{-1})

Functional groups	Chitin	Chitosan
–OH and –NH stretching	3441 (amide)	3433 (amide + amine)
–CH (CH_3) stretching	3109	3181
–CH (CH_2) stretching	2928	3005
C=O (amide) stretching	1659	1640
–NH (2º amide) bending	1562	1560
–CH (CH_3) bending	1425	1414
C–O stretching (s)	1157	1130
–C–O–C– (glycosidic linkage)	1030	1020

The glucosamine units are responsible for the similarities in the IR spectra of chitin and chitosan and according to Peter (1995), the slight differences in the spectra of chitin and chitosan arise from interactions such as van der Waals forces and possibly hydrogen bonding created by the amino groups (Kumari and Rath, 2014). As a result of the similarities and the incomplete conversion of chitin to chitosan, the degree of deacetylation (DDA) of chitin was determined. It has been shown that DDA above 50% signifies that more than half of the biopolymer chitin has been successfully converted to chitosan and therefore be suitable for use (Ghannam *et al.*, 2016). Following the

procedure of Domszy and Roberts (2010), they obtained 55% DDA while in this work 56.03% DDA was obtained.

Chitosan–Porphyrin Composite, (CPC)

The prepared CPC were translucent and purple in colour except for C-TPPS and its metallated series which were light brown. They were insoluble in water but soluble in 1% (v/v) acetic acid which was used to obtain their UV-Vis spectra (SI-2). The general features of the porphyrin spectra were retained, having an intense Soret band and weak Q-bands. Profile retention indicates that the electronic properties of the porphyrin were not lost due to composite formation. Other features observed were – (i) broadening of the bands, (ii) shifting of bands and (iii) little or no change in the spectra (Figure 4). Pronounced broadening of the porphyrin bands is indicative of aggregation and the broader the bands the greater the aggregation (Koti *et al.,* 2003). The 22 conjugated π–electrons of porphyrins cause a strong π–π interaction which facilitates the formation of aggregates (Pasternack *et al*., 1972). A blue shift is evidence of the formation of H–aggregates, while a red shift is for J-aggregation. There are instances aggregation without definate geometry, here only the broadening of the bands is observed with no significant shift in peaks (White 1978; Rubires 1999).

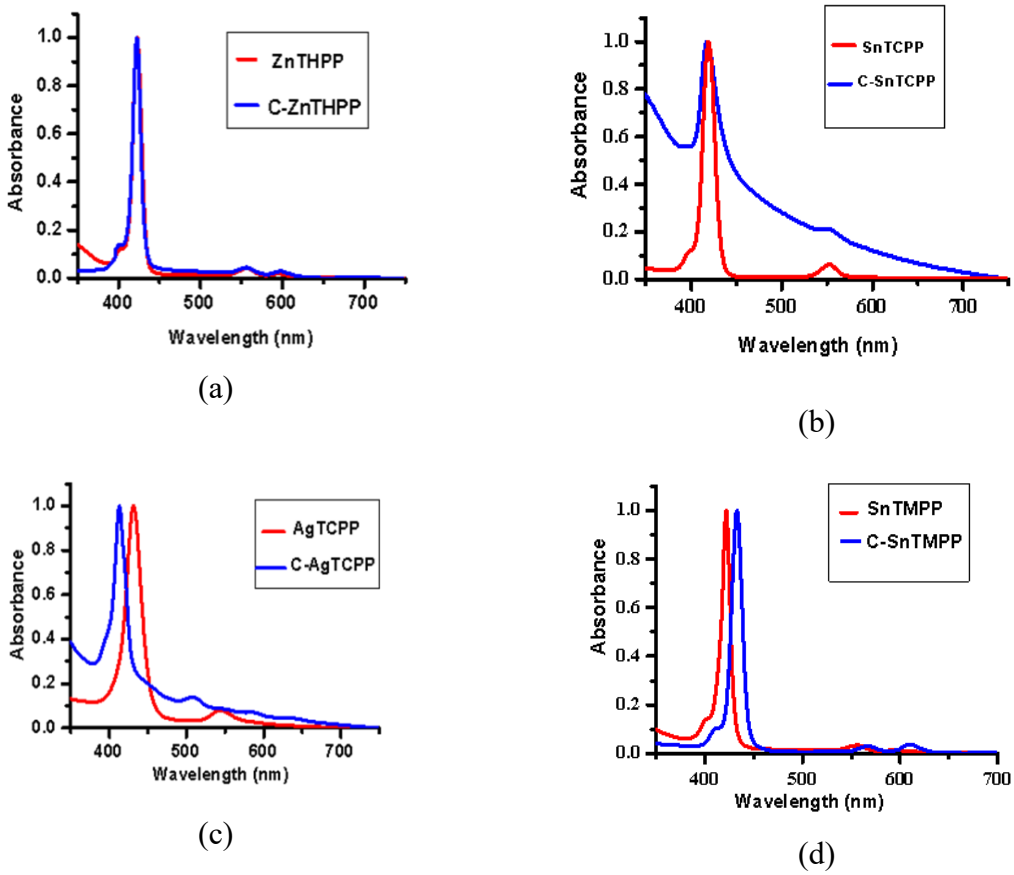

Figure 4: Some of the UV-Vis spectra of porphyrin and it CPC (a) no shift (b) broaden with no shift (c) blue shift (d) red shift

The slight shifts in the absorption bands are attributed to the interaction between the porphyrin unit and the chitosan either by electrostatic, hydrogen bonding and/or other van der Waal forces (Fontana *et al*., 2008). In addition, there is a possibility of the π-conjugated electron cloud of the porphyrin rings interacting with the hydroxyl groups of chitosan (Fontana *et al*., 2008). Table 2 is a classification of the CPCs based on the features described above.

Table 2: Classification of CPCs

Spectra Features	Chitosan-Porphyrin Composites (CPCs)
Band broadening	C-TPP series, C-TCPP series, C-TPPS, C-TMPP & C-ZnTMPP, C-TMPyP C-SnTMPyP
Band shift	C-TPPS, C-TCPP & C-AgTCPP, C-TMPP & C-SnTMPP, C-TMPyP
Little/no shift change	C-TPP series, C-MTPPS (M=Zn, Sn, Ag), C-THPP series, C-MTCPP (M=Z Sn), C-M'TMPyP (M'=Zn, Sn, Ag), C-MTMPP (M=Zn, Ag)

The FTIR data of the CPCs (SI-3) showed no newly created bonds in the CPC since no new bands were detected. Nevertheless, due to weak interactions between the two molecules, certain bands in the spectra of either chitosan or porphyrin shifted to new wavenumber. The chitosan bands that were impacted included the -OH/-NH, -CH (sp^3), -C=O stretching, and NH-bending vibrations. At the same time, affected bands of the porphyrin ring were the =CH and C=N stretching. The spectra revealed that the porphyrins' =CH stretching and -C=N vibrational frequencies occurred at lower wavenumbers in the CPC. Similarly, the composites exhibited the -N-H bending vibration of chitosan at a lower wavenumber. Nevertheless, in contrast to all free-base porphyrin composites, the -OH/-NH stretching vibration of chitosan was found to be at a higher wavenumber in a few metalloporphyrin composites (C-AgTMPyP, C-ZnTMPyP, C-ZnTPP, C-SnTPP, C-AgTPPS, and C-SnTHPP). One possible mechanism by which metal ions attach to chitosan macromolecules is electrostatic interaction with the oxygen atoms that are rich in electrons in the polar hydroxyl, or coordination to the nitrogen in the $-NH_2$ groups (Kumari and Rath, 2014). Possibly, the lower vibrational frequencies were a result of the metals' attachments to chitosan.

The Antimicrobial Inhibition Profile of Chitosan-Porphyrin Composites (CPCs)

Screening Exercise

The cumulative mean data of the antimicrobial inhibition profiles is shown in Table 3. *Staphylococcus aureus* was the most susceptible bacterium while *P. mirabilis* was the most recalcitrant. Chitosan showed antibacterial activity against all the tested pathogens with significant APDT action against *P. mirabilis*. Contrary to expectations, the antibacterial characteristics of the CPCs decreased when porphyrins were immobilized on chitosan, as opposed to when either chitosan or porphyrins were utilized independently (Daramola *et al.*, 2021; George *et al.*, 2022). The phytotoxic species needed for biocidal effect may be less abundant in the CPCs, which could justify this challenge. The substituents and metals present in each porphyrin molecule could induce diverse interactions with chitosan, which in turn potentially contribute to the observed decrease in photoactivity.

High positive charge density has been attributed to be one of the factors that increase the antibacterial activity of chitosan due to stronger electrostatic interaction between chitosan and the surface of the bacteria (Tweedy, 1964). It is for this reason that despite the decrease in antibacterial activity in the composites, the C-TMPyP series' zones of inhibition were larger than those without chitosan (George *et al*., 2022) except in the case of C-TMPyP and C-SnTMPyP. The impact of high positive charged density was also evident with the negatively charged porphyrins (C-TPPS and C-TCPP series) as these materials exhibited a significant decrease in bactericidal activities compared to their counterpart without chitosan (George *et al*., 2022).

Table 3: Zones of inhibition (mm) of the chitosan-porphyrin composites

	***Staphylococcus* sp.**		***Klebsiella* sp.**		***Proteus* sp.**		***E. coli***	
Strepto.	35 ± 1.4		27 ± 2.8		27 ± 1.4		35 ± 2.8	
	Dark	**Light**	**Dark**	**Light**	**Dark**	**Light**	**Dark**	**Light**
Chitosan	16 ± 0.7	25 ± 3.9	21 ± 1.0	27 ± 3.2	0	27 ± 2.8 (**B**)	17 ± 0.6	20 ± 1.4
TPP SERIES								
C-TPP	0	15 ± 0.7	0	0	0	0	0	15 ± 0.6
C-ZnTPP	0	0	0	0	0	0	0	0
C-SnTPP	0	0	0	0	0	0	0	0
C-AgTPP	14 ± 0.5	13 ± 0.0	0	12 ± 0.0	0	0	0	13 ± 0.7
TPPS SERIES								
C-TPPS	0	16 ± 1.4	0	15 ± 0.6	0	0	0	14 ± 2.8
C-ZnTPPS	18 ± 0.0	21 ± 0.7	11 ± 0.	0	0	0	13 ± 0.7	13 ± 1.4
C-SnTPPS	0	0	0	0	0	0	0	0
C-AgTPPS	0	0	13 ± 1.4	16 ± 0.7	0	0	0	0
THPP SERIES								
C-THPP	0	0	0	0	0	0	0	0
C-ZnTHPP	16 ± 2.8	21 ± 2.1	0	0	0	0	0	0
C-SnTHPP	0	0	0	0	0	0	0	0
C-AgTHPP	14 ± 0.0	20 ± 1.4	15 ± 0.	16 ± 0.0	0	13 ± 1.4	13 ± 0.0	14 ± 0.0
TCPP SERIES								
C-TCPP	0	0	0	0	0	0	0	0
C-ZnTCPP	0	12 ± 0.0	0	0	0	0	0	0
C-SnTCPP	14 ± 0.7	23 ± 1.4	12 ± 0.7	17 ± 0.7	0	0	0	0
C-AgTCPP	0	20 ± 1.4	0	0	0	0	0	0
TMPP SERIES								
C-TMPP	0	0	0	0	0	0	0	0
C-ZnTMPP	0	0	0	0	0	0	0	0
C-SnTMPP	0	0	0	0	0	0	0	0
C-AgTMPP	38 ± 0.0	39 ± 5.6	33 ± 0.7	36 ± 2.8	0	26 ± 3.5	36 ± 4.2	34 ± 2.8
TMPyP SERIES								
C-TMPyP	0	0	0	0	0	0	0	0
C-ZnTMPyP	0	16 ± 0.7	25 ± 1.4	25 ± 1.4	0	0	27 ± 1.4	16 ± 0.7
C-SnTMPyP	0	15 ± 0.7	13 ± 0.7	15 ± 0.7	0	0	0	0
C-AgTMPyP	37 ± 1.4	38 ± 1.4	33 ± 3.5	32 ± 0.7	0	0	25 ± 2.8	29 ± 2.1

B = Bacteriostatic Strepto. = streptomycin sulphate (84 mg/mL) photosensitizer (30 mg/mL)

For the neutral porphyrins (C-TPP, C-THPP, and C-TMPP series), increased activity occurred with the silver complexes. It is assumed that the effect of the chelation of silver by chitosan was responsible for their increased antibacterial properties. Chitosan has been reported to have high chelating capacity for metals being one of its modes of antimicrobial action (Yilmaz Atay, 2019). This was possible with the silver complexes because the silver metal ion is sitting-atop in the porphyrin cavity and therefore easily accessible for chelation which is in line with the Chelating theory (Tweedy 1964).

In most cases where biocidal activity was observed, both dark toxicity and phototoxicity were present. However, certain CPCs exhibited phototoxicity without dark toxicity. These included C-TPP, C-TPPS, C-ZnTCPP, C-AgTCPP, C-ZnTMPyP, and C-SnTMPyP against *S. aureus*; C-AgTPP and C-TPPS against *K. pneumoniae*; C-AgTHPP and C-AgTMPP against *P. mirabilis*; and C-TPP, C-AgTPP, and C-TPPS against *E. coli*.

Determination of MIC and MBC

From a previous screening exercise using SnTCPP, SnTHPP, ZnTCPP, ZnTHPP, ZnTPPS, (Daramola *et al.*, 2021; George *et al.*, 2022) and in this current study, C-AgTHPP, and C-AgTMPP were deemed suitable for MBC and MIC testing since they exhibited APDT activity against all four pathogens. Table 4 showcases the responses of the pathogens to the three concentrations of the photosensitizers. SnTCPP and ZnTCPP showed no growth inhibition therefore, the MIC and MBC values are likely greater than 5.0 µg/mL. SnTHPP, had MBC values at 5.0 µg/mL against three of the bacterial isolates (*E. coli, P. mirabilis*, and *S. aureus*). ZnTPPS recorded MBC values against two of the bacterial isolates namely, *K. pneumoniae* and *S. aureus* at 5.00 µg/mL and 2.50 µg/mL respectively. ZnTHPP had one against *S. aureus* at 2.5 µg/mL Worthy of note is the MBC values for C-AgTHPP and C-AgTMPP were active at the lowest concentration (1.25 µg/mL) against all the bacterial isolates with the exception of *P. mirabilis*, with an MBC value for C-AgTHPP at 5.0 µg/mL.

Table 4. Minimum Inhibitory Concentration (MIC) and Minimum Bactericidal Concentration (MBC) values of porphyrin complexes and CPCs at the concentrations of 5.0, 2.5, 1. 25 µg/mL.

Porphyrin Compounds	Concentrations (µg/mL)	Bacterial Isolates			
		Escherichia coli	*Klebsiella pneumoniae*	*Proteus mirabilis*	*Staphylococcus aureus*
SnTCPP	5	+	+	+	+
	2.5	+	+	+	+
	1.25	+	+	+	+
ZnTCPP	5	+	+	+	+
	2.5	+	+	+	+
	1.25	+	+	+	+
ZnTHPP	5	+	+	+	-
	2.5	+	+	+	-*
	1.25	+	+	+	+
ZnTPPS	5	+	-*	+	-
	2.5	+	+	+	-*
	1.25	+	+	+	+
SnTHPP	5	-*	+	-*	-*
	2.5	+	+	+	+
	1.25	+	+	+	+
C–AgTHPP	5	–	–	-*	–
	2.5	–	–	+	–
	1.25	-*	-*	+	-*
C–AgTMPP	5	–	–	–	–
	2.5	–	–	–	–
	1.25	-*	-*	-*	-*

$+ \Rightarrow$ Growth : $- \Rightarrow$ no Growth : $- * \Rightarrow$ MBC

Rate of Kill Assay

After 24 hours of incubation, all bacterial isolates were eliminated in the time-kill assay, which was conducted using each of the PSs MBC values obtained against each isolate (Figure 5). Figure 5a shows that by the 18th hour, five of the tested PSs had eliminated *S. aureus*, and by the 24th hour, the C-AgTHPP had shown full bactericidal action. The results demonstrated that the three active PSs MBC concentrations tested had complete or near-complete bactericidal efficacy against *K. pneumoniae* (Figure 5b). Figure 5c showed that other PSs had effectively eliminated the *E. coli*

cells at the 18th hour, whereas C-AgTHPP exhibited a delayed rate of kill (between the 18th and 24th hour). Within the first 18 hours of incubation, none of the three PSs MBC values of *P. mirabilis* had a complete bactericidal effect. However, by the 24th hour of incubation, the effect of the CPCs became apparent (Figure 5d).

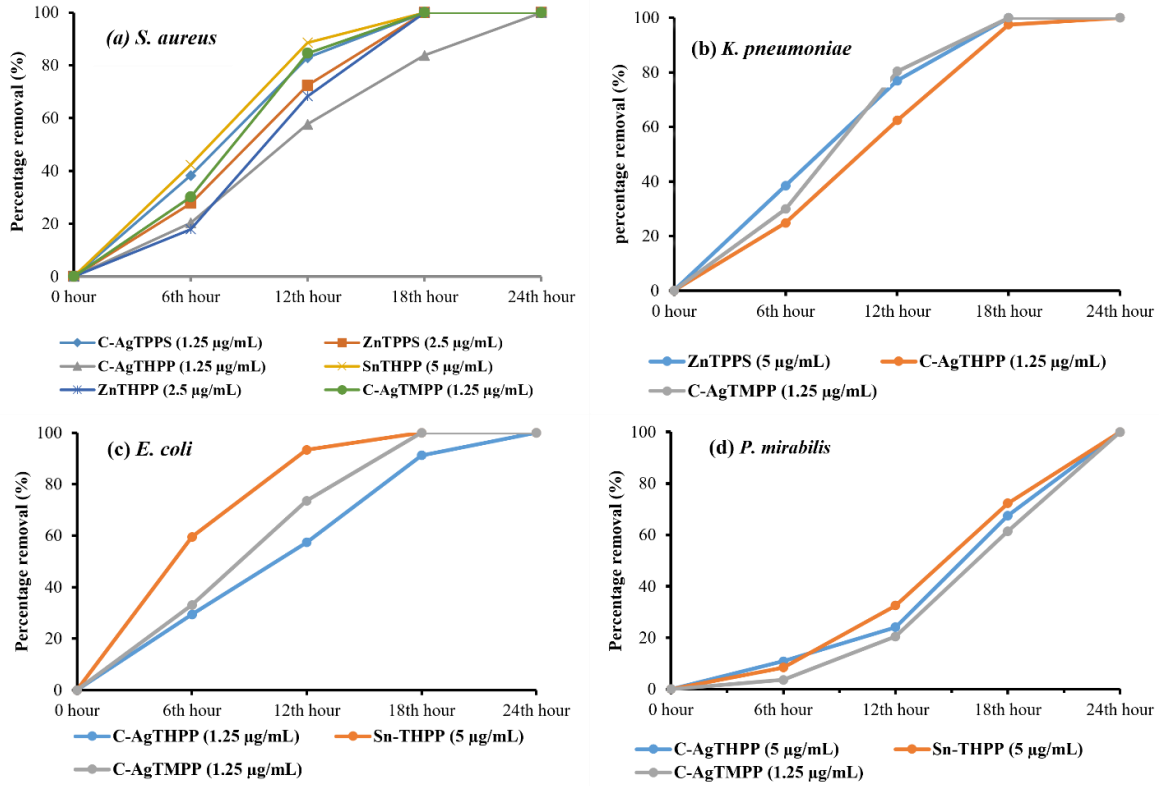

Figure 5: Rate of Kill of C-AgTHPP, C-AgTMPP and Sn-THPP against (a) *S. aureus* (b) *K. pneumoniae* (c) *E. coli* (d) *P. mirabilis*

CONCLUSION

We created and studied a chitosan film that included both free-base porphyrins and metalloporphyrins. *S. aureus, K. pneumoniae, P. mirabilis,* and *E. coli* were eliminated after 24 hours at extremely low concentrations by the phototoxicity action of silver *meso*-tetra(4-hydroxylphenyl) porphyrin-chitosan composites (C-AgTMPP) and silver *meso*-tetra(4-hydroxylphenyl) porphyrin-chitosan composite (C-AgTHPP). Our study has shown that C-AgTMPP can be more effective as an APDT against these wound pathogens when combined with cheap and non-toxic chitosan. There may be no need for photodynamic therapy as some data in this study confirmed dark toxicity for some CPCs. These results show that APDT will be easier to implement for localized infection and might pave the way for less complicated wound management using sunlight and the CPC photosensitizers. However, to establish an effective protocol, additional research is required to identify the ideal dosage for accomplishing total elimination with APDT, along with defining certain light characteristics (light treatment intensity and duration) and this further study is expected to be mostly an *in vivo* evaluation.

REFERENCES

Abbaspour, M., Sharif Makhmalzadeh, B., Rezaee, B., Shoja, S., and Ahangari, Z. (2015). Evaluation of the Antimicrobial Effect of Chitosan/Polyvinyl Alcohol Electrospun Nanofibers Containing Mafenide Acetate. *Jundishapur Journal of Microbiology*, 8(10) 167 - 185.

Abrahamse, H., and Hamblin, M. R. (2016). New photosensitizers for photodynamic therapy. *The Biochemical Journal*, 473(4), 347–364.

Almenara-Blasco M., Pérez-Laguna V., Navarro-Bielsa A., Gracia-Cazaña T. and Gilaberte Y. (2024). Antimicrobial photodynamic therapy for dermatological infections: current insights and future prospects. *Frontiers in Photobiology,* 2, 1-13.

Alshareef, F. (2021). Protocol to Evaluate Antibacterial Activity MIC, FIC and Time Kill Method. *Acta Scientific Microbiology*, 4(5), 02–06.

Alves, E., Costa, L., Carvalho, C. M., Tomé, J. P., Faustino, M. A., Neves, M. G., Tomé, A. C., Cavaleiro, J. A., Cunha, Â., and Almeida, A. (2009). Charge effect on the photoinactivation of Gram-negative and Gram-positive bacteria by cationic meso-substituted porphyrins. *BMC Microbiology*, 9(1), 70.

Andrews, J. M. (2001). Determination of minimum inhibitory concentrations. *The Journal of Antimicrobial Chemotherapy*, 48 *Suppl 1*, 5–16.

Atiyeh, B. S., Dibo, S. A., and Hayek, S. N. (2009). Wound Cleansing, Topical Antiseptics and Wound Healing. *International Wound Journal*, 6(6), 420–430.

Bonnett, R., McGarvey D. J., Harriman, A., Land, E. J., Truscott, T. G., and Winfield, U.-J. (1988). Photophysical Properties of meso-Tetraphenylporphyrin and Some meso-Tetra(Hydroxyphenyl) porphyrins, *Photochemistiy and Photobiology*, 48(3), 271-276.

Buchovec, I., Lukseviciute, V., Marsalka, A., Reklaitis, I., and Luksiene, Z. (2016). Effective photosensitization-based inactivation of Gram (−) food pathogens and molds using the chlorophyllin–chitosan complex: Towards photoactive edible coatings to preserve strawberries. *Photochemical & Photobiological Sciences*, 15(4), 506–516.

Caminos, D. A., Spesia, M. B., Pons, P., and Durantini, E. N. (2008). Mechanisms of Escherichia coli photodynamic inactivation by an amphiphilic tricationic porphyrin and 5,10,15,20-tetra(4-N,N,N-trimethylammoniumphenyl) porphyrin. *Photochemical & Photobiological Sciences: Official Journal of the European Photochemistry Association and the European Society for Photobiology*, *7*(9), 1071–1078.

Castro, K. A. D. F., Moura, N. M. M., Figueira, F., Ferreira, R. I., Simões, M. M. Q., Cavaleiro, J. A. S., Faustino, M. A. F., Silvestre, A. J. D., Freire, C. S. R., Tomé, J. P. C., Nakagaki, S., Almeida, A., and Neves, M. G. P. M. S. (2019). New Materials Based on Cationic Porphyrins Conjugated to Chitosan or Titanium Dioxide: Synthesis, Characterization and Antimicrobial Efficacy. *International Journal of Molecular Sciences*, 20(10), 1 - 21.

Daramola, O. B., Olajide, A. A., Torimiro, N., and George, R. C. (2021). Antibacterial Photodynamic Therapeutic Studies of Metallated Porphyrin against Chronic Wound Colonising Bacterial Isolates. *Journal of Chemical Society of Nigeria*, 46(2), 366-368

Domszy, J. G., and Roberts, G. A. F. (1985). Evaluation of infrared spectroscopic techniques for analysing chitosan. *Die Makromolekulare Chemie*, 186(8), 1671–1677.

Fayyaza, F., Rahimi, R., and Rassa, M. (2016). Preparation of Photo-Bactericidal Cellulosic Fabrics Impregnated with Tetra- Cationic Porphyrin Compounds. *Journal of Antimicrobial Agents*, 02(04), 1–4.

Feese, E., Sadeghifar, H., Gracz, H. S., Argyropoulos, D. S., and Ghiladi, R. A. (2011). Photobactericidal porphyrin-cellulose nanocrystals: Synthesis, characterization, and antimicrobial properties. *Biomacromolecules*, 12(10), 3528–3539.

Fontana, C. R., dos Santos Junior, D. S., Bosco, J. M., Spolidorio, D. M., and Chiérici Marcantonio, R. A. (2008). Evaluation of Chitosan Gel as Antibiotic and Photosensitizer Delivery. *Drug Delivery*, 15(7), 417–422.

George, R. C., Torimiro, N., Daramola, O. B., and Olajide, A. A. (2022). Zinc, Tin and Silver Porphyrins (TPP, TCPP, TMPP, THPP, TPPS, TMPyP) as photosensitizers in antibacterial photodynamic therapy for chronic wounds: A screening study. *Ethiopian Journal of Science and Technology*, 15(2), 187–207.

Gouterman, M. (1978.) Optical Spectra and Electronic Structure of Porphyrin and Related Rings. The Porphyrins. Dolphin, D. [Ed.], New York: Academic, vol 3, pp 1-11.

Ghannam, H. E., S. Talab, A., V. Dolgano, N., M.S. Husse, A., and Abdelmagui, N. M. (2016). Characterization of Chitosan Extracted from Different Crustacean Shell Wastes. *Journal of Applied Sciences*, 16(10), 454–461.

Gourlot, C., Gosset, A., Glattard, E., Christopher Aisenbrey, C., Rangasamy, S., Rabineau, M., Ouk, T.-S., Sol, V., Lavalle, P., Gourlaouen, C., Ventura, B., Bechinger, B., and Heitz, V. (2022). Antibacterial Photodynamic Therapy in the Near-Infrared Region with a Targeting Antimicrobial Peptide Connected to a π-Extended Porphyrin. *ACS Infectious Diseases*, 8(8) 1509-1520

Gyulkhandanyan, G. V., Paronyan, M. H., Hovsepyan, A. S., Ghazaryan, R. K., Tovmasyan, A. G., Gyulkhandanyan, A. G., Gyulkhandanyan, A. G., and Amelyan, G. V. (2016). Photodynamic inactivation of Gram (-) and Gram (+) microorganisms by cationic porphyrins and metalloporphyrins. *Proceeding of SPIE,* 7380, 1-2.

Harding, K. G., Morris, H. L., and Patel, G. K. (2002). Science, medicine and the future: Healing chronic wounds. *BMJ (Clinical Research Ed.)*, 324(7330), 160–163.

Hoang, T. P. N., Ghori, M. U., Ousey, K. J., and Conway, B. R. (2022). Current and advanced therapies for chronic wound infection. *Pharmaceutical Journal*, 309(7963), 1–27.

Huang, L., Huang, Y.-Y., Mroz, P., Tegos, G. P., Zhiyentayev, T., Sharma, S. K., Lu, Z., Balasubramanian, T., Krayer, M., Ruzié, C., Yang, E., Kee, H. L., Kirmaier, C., Diers, J. R., Bocian, D. F., Holten, D., Lindsey, J. S., and Hamblin, M. R. (2010). Stable Synthetic Cationic Bacteriochlorins as Selective Antimicrobial Photosensitizers. *Antimicrobial Agents and Chemotherapy*, 54(9), 3834-3841.

Ji, H., Dong, T., Liang, G., Xu, H., Wang, C., Liu, T., and Hong G. (2023). Evaluation of Antibacterial Effect of a Cationic Porphyrin Derivative on *Pseudomonas aeruginosa* in Photodynamic Therapy. Photodiagnosis and Photodynamic Therapy 44, 10385 -103872

Karaoğlu G. E., Aydın Z. U., Erdönmez D., Göl C., and Durmuş M., (2020). Efficacy of antimicrobial photodynamic therapy administered using methylene blue, toluidine blue and

tetra 2-mercaptopyridine substituted zinc phthalocyanine in root canals contaminated with *Enterococcusaecalis*, *Photodiagnosis and Photodynamic Therapy,* 32, 102038

Koti, A. S. R., Taneja, J., and Periasamy, N. (2003). Control of coherence length and aggregate size in the J-aggregate of porphyrin. *Chemical Physics Letters*, *375*(1), 171–176.

Kou, J., Dou, D., and Yang, L. (2017). Porphyrin photosensitizers in photodynamic therapy and its applications. *Oncotarget*, 8(46), 81591–81603.

Král, V., Rusin, O., Charvátová, J., Anzenbacher, P., and Fogl, J. (2000). Porphyrin phosphonates: Novel anionic receptors for saccharide recognition. *Tetrahedron Letters*, 41(51), 10147–10151.

Kumari, S., and Rath, P. K. (2014). Extraction and Characterization of Chitin and Chitosan from (Labeo rohit) Fish Scales. *Procedia Materials Science*, *6*, 482–489.

Lakowicz, J. R. (Ed.). (2006). *Principles of Fluorescence Spectroscopy*. Springer US.

Liu, Y., Qin, R., Zaat, S. A. J., Breukink, E., and Heger, M. (2015). Antibacterial photodynamic therapy: Overview of a promising approach to fight antibiotic-resistant bacterial infections. *Journal of Clinical and Translational Research*, 1(3), 140–167.

Majekodunmi, S. O. (2016). Current Development of Extraction, Characterization and Evaluation of Properties of Chitosan and Its Use in Medicine and Pharmaceutical Industry. *American Journal of Polymer Science*, 6(3), 86–91.

Milanesio, M. E., Alvarez, M. G., Yslas, E. I., Borsarelli, C. D., Silber, J. J., Rivarola, V., and Durantini, E. N. (2001). Photodynamic studies of metallo 5,10,15,20-tetrakis(4-methoxyphenyl) porphyrin: Photochemical characterization and biological consequences in a human carcinoma cell line. *Photochemistry and Photobiology*, 74(1), 14–21.

Okur, M. E., Karantas, I. D., Şenyiğit, Z., Üstündağ Okur, N., and Siafaka, P. I. (2020). Recent trends on wound management: New therapeutic choices based on polymeric carriers. *Asian Journal of Pharmaceutical Sciences*, 15(6), 661–684.

Ongarora, B. G. (2022). Recent technological advances in the management of chronic wounds: A literature review. *Health Science Reports*, 5(3), e641.

Ormond A. B. and Freeman H. S. (2013) Dye sensitizers for photodynamic therapy. *Materials,* 6, 817-840

Pasternack, R. F., Huber, P. R., Boyd, P., Engasser, G., Francesconi, L., Gibbs, E., Fasella, P., Cerio Venturo, G., and Hinds, L. deC. (1972). Aggregation of meso-substituted water-soluble porphyrins. *Journal of the American Chemical Society*, 94(13), 4511–4517.

Peter, M. G. (1995). Applications and Environmental Aspects of Chitin and Chitosan. *Journal of Macromolecular Science, Part A*, 32(4), 629–640.

Prasanth, C. S., Karunakaran, S. C., Paul, A. K., Kussovski, V., Mantareva, V., Ramaiah, D., Selvaraj, L., Angelov, I., Avramov, L., Nandakumar, K., and Subhash, N. (2014). Antimicrobial photodynamic efficiency of novel cationic porphyrins towards periodontal

Gram-positive and Gram-negative pathogenic bacteria. *Photochemistry and Photobiology*, 90(3), 628–640.

Raafat, D., von Bargen, K., Haas, A., and Sahl, H.-G. (2008). Insights into the Mode of Action of Chitosan as an Antibacterial Compound. *Applied and Environmental Microbiology*, 74(12), 3764–3773.

Ranjbar, R., and Takhtfooladi, M. A. (2016). The effects of photobiomodulation therapy on Staphylococcus aureus infected surgical wounds in diabetic rats. A microbiological, histopathological, and biomechanical study. *Acta Cirurgica Brasileira*, 31(8), 498–504.

Rubires R., Crusats J., El-Hachemi Z., Jaramillo T., López M., Valls E., Farrera J.-A., and Ribó J. M. (1999), Self-assembly in water of the sodium salts of *meso*-sulfonatophenyl substituted porphyrins, *New Journal Chemistry,* 23, 189-198

Savelyeva, I. O., Zhdanova, K.A., Gradova, M.A., Gradov, O.V., and Bragina, N.A. (2023). Cationic Porphyrins as Antimicrobial and Antiviral Agents in Photodynamic Therapy. *Current Issues in Molecular Biology.* 45, 9793–9822.

Shrestha, A., Cordova, M., and Kishen, A. (2015). Photoactivated polycationic bioactive chitosan nanoparticles inactivate bacterial endotoxins. *Journal of Endodontics*, 41(5), 686–691.

Shrestha, A., Hamblin, M. R., and Kishen, A. (2012). Characterization of a conjugate between Rose Bengal and chitosan for targeted antibiofilm and tissue stabilization effects as a potential treatment of infected dentin. *Antimicrobial Agents and Chemotherapy*, 56(9), 4876–4884.

Tominaga, T. T., Yushmanov, V. E., Borissevitch, I. E., Imasato, H., and Tabak, M. (1997). Aggregation phenomena in the complexes of iron tetraphenylporphine sulfonate with bovine serum albumin. *Journal of Inorganic Biochemistry*, 65(4), 235–244.

Tsai, G. J., and Su, W. H. (1999). Antibacterial activity of shrimp chitosan against *Escherichia coli. Journal of Food Protection*, 62(3), 239–243.

Tsai, T., Chien, H.-F., Wang, T.-H., Huang, C.-T., Ker, Y.-B., and Chen, C.-T. (2011). Chitosan Augments Photodynamic Inactivation of Gram-Positive and Gram-Negative Bacteria. *Antimicrobial Agents and Chemotherapy*, 55(5), 1883–1890.

Tweedy, B. G. (1964). Plant extracts with metal ions as potential antimicrobial agents. *Phytopathology*, 55, 910–914.

Vilela, S. F. G., Junqueira, J. C., Barbosa, J. O., Majewski, M., Munin, E., and Jorge, A. O. C. (2012). Photodynamic inactivation of Staphylococcus aureus and Escherichia coli biofilms by malachite green and phenothiazine dyes: An in vitro study. *Archives of Oral Biology*, 57(6), 704–710.

Viola, G., and Dall'Acqua, F. (2006). Photosensitization of biomolecules by phenothiazine derivatives. *Current Drug Targets*, 7(9), 1135–1154.

White W. I. (1978), Aggregation of porphyrins and metalloporphyrins. In: The Porphyrins, D. Dolphin (ed.), Academic Press, New York, vol. 5, pp. 303-339

Woodburn, K., Chang, C. K., Lee, S., Henderson, B., and Kessel, D. (1994). Biodistribution and PDT efficacy of a ketochlorin photosensitizer as a function of the delivery vehicle. *Photochemistry and Photobiology*, *60*(2), 154–159.

Yilmaz Atay. H. (2019). Antibacterial Activity of Chitosan-Based Systems. *Functional Chitosan*, 457–489.

Zhang, J., Yuan, X., Li, H. Zhang, Y., Pang, K., Sun, C., Liu, Z., Li, J., Ma, L., Song, J., and Chen L. (2024). Novel Porphyrin Derivative containing Cations as New Photodynamic Antimicrobial Agent with High Efficiency, *RSC Advances*, 14(5), 3122-3134.

Zhang, X., Shu, W., Yu, Q., Qu, W., Wang, Y., and Li, R. (2020). Functional Biomaterials for Treatment of Chronic Wound. *Frontiers in Bioengineering and Biotechnology*, *8*, 516.

Zhu, Wang, Q., Lu, S., and Niu, Y. (2017). Hydrogen Peroxide: A Potential Wound Therapeutic Target? *Medical Principles and Practice*, *26*(4), 301–308.

Zvezdova, D. (2010). Synthesis and characterization of chitosan from marine sources in Black Sea. *Annual Proceedings*, *49*, 65–69.

SUPPLEMENTARY INFORMATION (SI)

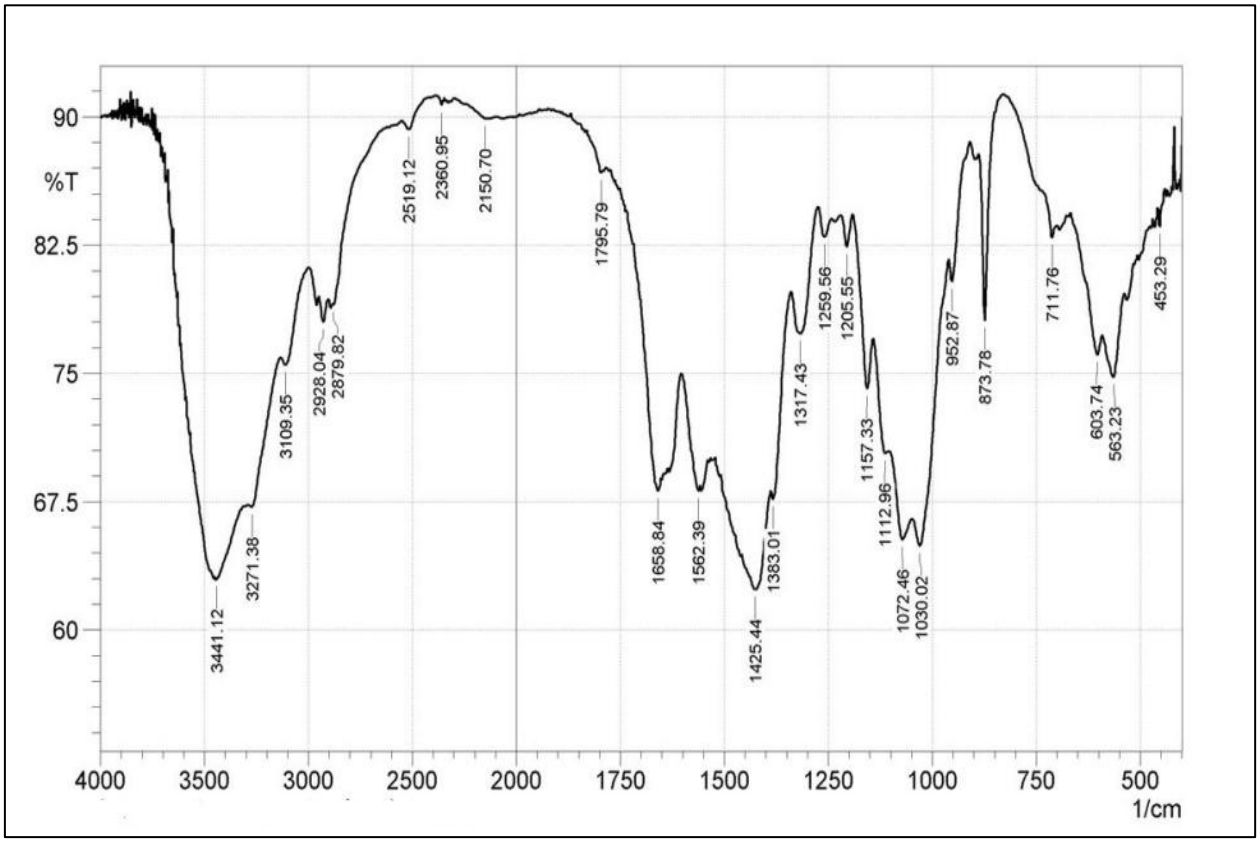

a.

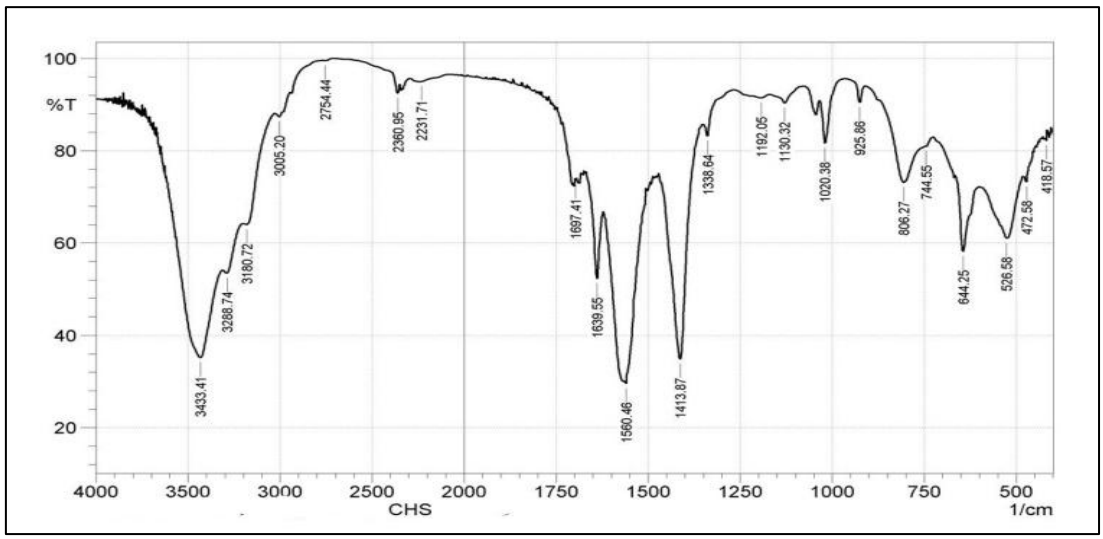

b.

SI-1: Infra-red spectrum of (a) Chitin (b) Chitosan

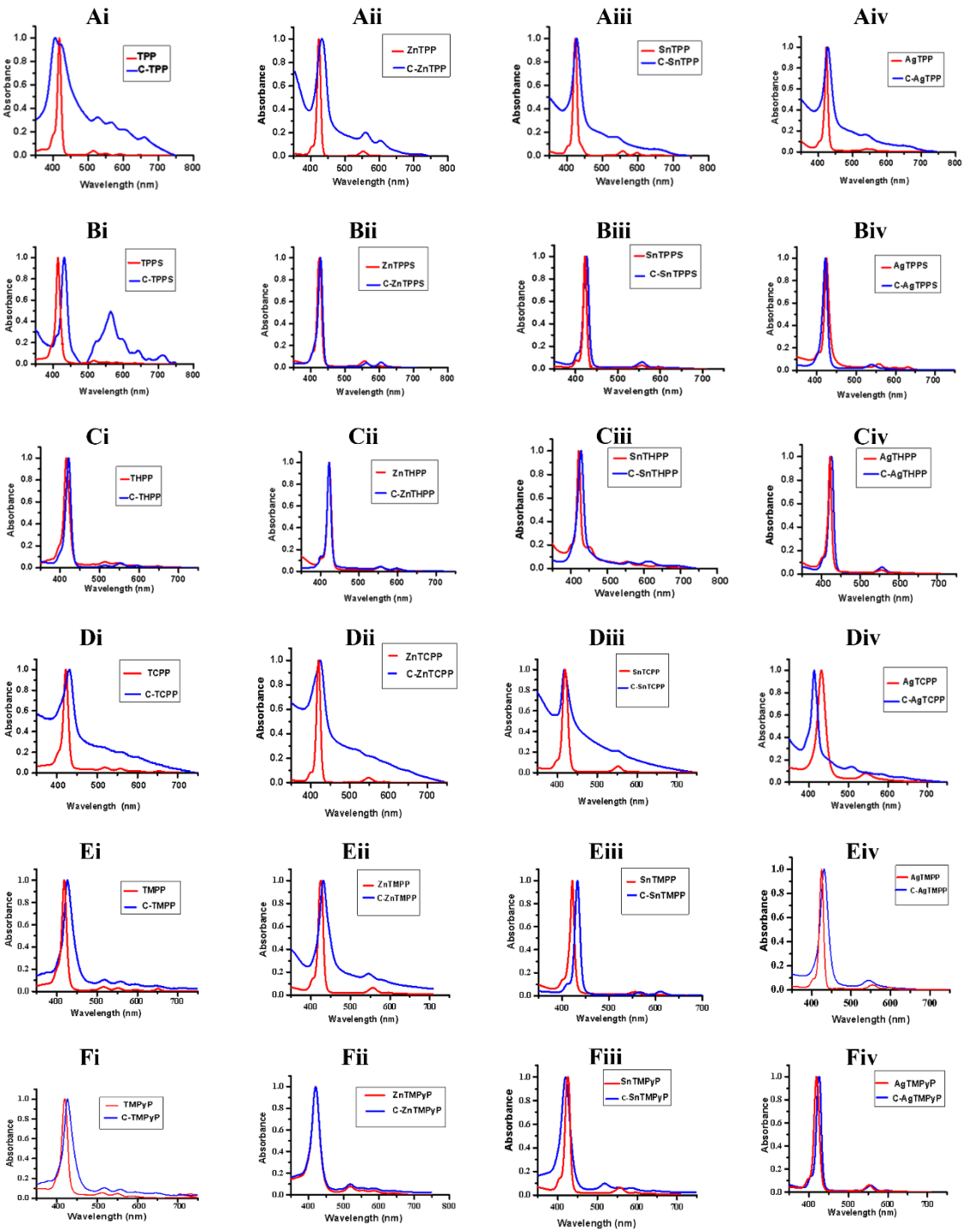

SI-2: Electronic spectra of CPC series (A) TPP and MTPP (B) TPPS and MTPPS (C) THPP and MTHPP (D) TCPP and MTCPP (E) TMPP and MTMPP (F) TMPyP and MTMPyP (The Blue line represents the spectra of the porphyrins incorporated into the chitosan (CPC) while the red line is the spectra of the porphyrins only)

SI-3: FT-IR Data of the CPCs (KBr cm^{-})

TPP SERIES						
Functional groups	**CHITOSAN**	**TPP**	**C-TPP**	**C-ZnTPP**	**C-SnTPP**	**C-AgTPP**
–OH and –NH stretchi	3433	-------	3431	3441	3446	3430
–CH (sp^2)	-------	3090	2928	3267	3107	3174
–CH (CH_2) stretching	3005	-------	2855	-------	2928	-------
–NH (amide) bending	1560	-------	1560	1574	1558	1562
–C=O (amide) stretchi	1640	-------	1654	-------	1653	-------
–C=N stretching	-------	1358	1411	1346	1379	1339
TPPS SERIES						
Functional groups	**CHITOSAN**	**TPPS**	**C-TPPS**	**C-ZnTPPS**	**C-SnTPPS**	**C-AgTPPS**
–OH and –NH stretchi	3433	3421	3433	3428	3422	3447
–CH (sp^2)	-------	3052	3005	2928	2920	3271
–CH (CH_2) stretching	3005	-------	3180	2893	2888	2928
–NH (amide) bending	1560	-------	1560	1578	1576	1559
–C=O (amide) stretchi	1640	-------	1639	-------	1653	1653
–C=N stretching	-------	1350	1413	1340/1414	1411/1341	1418/1379
THPP SERIES						
Functional groups	**CHITOSAN**	**THPP**	**C-THPP**	**C-ZnTHPP**	**C-SnTHPP**	**C-AgTHPP**
–OH and –NH stretchi	3433	3415	3421	3404	3443	3431
–CH (sp^2)	-------	2928	2924	-------	2964	2926
–CH (CH_2) stretching	3005	-------	2855	-------	-------	-------
–NH (amide) bending	1560	-------	1560	1568	-------	1572
–C=O (amide) stretchi	1640	-------	1654	1653	1634	-------
–C=N stretching	-------	1410	1411	1410/1342	1410/1356	1408/1342
TMPP SERIES						

Functional groups	CHITOSAN	TMPP	C-TMPP	C-ZnTMPP	C-SnTMPP	C-AgTMP
–OH and –NH stretchi	3433	-------	3427	3422	3439	3422
–CH (sp^2)	-------	3003	2926	3021	2918	-------
–CH (CH_2) stretching	3005	-------	2889	2938	-------	-------
–NH (amide) bending	1560	-------	1560	1560	1597	1570
–C=O (amide) stretchi	1640	-------	1654	-------	1653	1655
–C=N stretching	-------	1350	1413	1414	1411	1418
TCPP SERIES						
Functional groups	**CHITOSAN**	**TCPP**	**C-TCPP**	**C-ZnTCPP**	**C-SnTCPP**	**C-AgTCP**
–OH and –NH stretchi	3433	------	3421	3424	3375	3375
–CH (sp^2)	-------	2655	2924	2928	2920	2920
–CH (CH_2) stretching	3005	-------	2855	2893	2884	2884
–NH (amide) bending	1560	-------	1560	1578	1570	1570
–C=O (amide) stretchi	1640	1694	1654	-------	1647	1647
–C=N stretching	-------	1406	1411	1414/1341	1412/1341	1412/1341
TMPyP SERIES						
Functional groups	**CHITOSAN**	**TMPyP**	**C-TMPyP**	**C-ZnTMPy**	**C-SnTMPy**	**C-AgTMPyP**
–OH and –NH stretchi	3433	-------	3433	3447	3424	3443
–CH (sp^2)	-------	3092	2924	2926	2926	2924
–CH (CH_2) stretching	3005	-------	2889	-------	-------	2859
–NH (amide) bending	1560	-------	1558	1549	1541	1541
–C=O (amide) stretchi	1640	-------	1635	1634	1649	1638
–C=N stretching	-------	1467	1417	1416/1385	1421/1384	1420/1384